Available online at www.sciencedirect.com
SCIENCE DIRECT
Sedimentary Geology 183 (2006) 203–216
Sedimentary Geology
www.elsevier.com/locate/sedgeo

Hydrothermal venting and basin evolution (Devonian, South China): Constraints from rare earth element geochemistry of chert

Daizhao Chen [a,*], Hairuo Qing [b], Xin Yan [a], He Li [a]

[a] Institute of Geology and Geophysics, Chinese Academy of Sciences, PO Box 9825, Beijing 100029, China
[b] Department of Geology, University of Regina, Regina, SK, Canada S4S 0A2

Received 12 May 2004; received in revised form 17 September 2005; accepted 20 September 2005

Abstract

This paper presents rare earth element (REE) geochemistry of siliceous deposits from which hydrothermal activity and basin evolution are elucidated, in the Late Devonian, in the Yangshuo basin, South China, where siliceous deposits widely occurred as nodular chert in the deep-water limestones and bedded chert interbeded with tuffaceous chert in the early Late Devonian. Both nodular and bedded cherts are characterized by very low La abundances (avg. 2.07 and 2.49 ppm, respectively), intermediate negative Ce anomalies (Ce/Ce*: avg. 0. 69 and 0.61), slight to intermediate positive Eu anomalies (Eu/Eu*: avg. 1.33 and 1.57), and low to intermediate shale-normalized La_n/Yb_n values (avg. 0.86 and 0.52) and intermediate La_n/Ce_n values (avg. 1.61 and 1.72). These suggest both nodular and bedded cherts formed in the open marine basin of South China, rather than in the intracontinental rift basin as previously assumed, with involvement both with seawaters as indicated by intermediate negative Ce anomalies and generally LREE-depleted patterns, and hydrothermal vent fluids as indicated by convex, less LREE-depleted patterns with apparent positive Eu anomalies. In comparison with nodular and bedded chert, the tuffaceous chert has the highest La abundances (avg. 17.11 ppm), similar ranges of Ce anomalies (avg. 0.63) and La_n/Ce_n values (avg. 1.77), but lower La_n/Yb_n values (avg. 0.48) and no apparent positive Eu anomalies (avg. 0.97). This suggests that the tuffaceous fallouts were also significantly modified by the hydrothermal fluid and seawater. Rapid spatial variations of Eu/Eu* values and degree of LREE-depletions in the studied basin are recognized, characterizing a spatially differential hydothermal activity that is not well discriminated by major element features. Such a difference in hydrothermal activity is interpreted as having been related to the intensity and depth of syndepositional tectonic activity, reconciling the structural pattern unraveled by stratigraphic packages.

Keywords: REE patterns; Chert; Hydrothermal activity; Basin evolution; Open marine basin; Late Devonian; South China

1. Introduction

Rare earth elements (REE) in chert, because of their immobility during the diagenesis (Murray et al., 1992), have been commonly used as important geochemical indicators to assess the depositional environments and paleogeography of oceans (Shimizu and Masuda, 1977; Murray et al., 1990, 1991; Murray,

* Corresponding author. Tel.: +86 10 62008092; fax: +86 10 62010846.
E-mail addresses: dzh-ch@mail.igcas.ac.cn (D. Chen), hairuo.qing@uregina.ca (H. Qing).

0037-0738/$ - see front matter © 2005 Elsevier B.V. All rights reserved.
doi:10.1016/j.sedgeo.2005.09.020

1994; Ding and Zhong, 1995; Armstrong et al., 1999; Owen et al., 1999), which commonly cannot be unequivocally specified merely upon petrographic and physical signatures. Thus, the chert, although of minor significance in stratigraphic records, can provide critical information of paleoceanographic and tectonic evolutions (e.g., Murray et al., 1991; Holser, 1997). The REE behaviours of hydrothermal vent fluids and sediment particulates in active ocean ridge system have been extensively and well documented, i.e., apparent positive Eu anomalies (Michard et al., 1983; Michard, 1989; German et al., 1990, 1999; Douville et al., 1999). Nevertheless, rare REE data on which the chert derived from hydrothermal activity were unambiguously evident in the geological records.

Siliceous deposits, which locally host manganese deposits in southern Guangxi (Wu et al., 1987; Tang et al., 1994), are widely distributed in the Devonian (particularly the Frasnian) interplatform basinal successions, which were deposited in the elongate interplatform basins (or troughs), in the Guangxi–Hunan area, South China (Fig. 1A) (Wu et al., 1987). Although a few studies of the chert were undertaken in the areas south and west of Guangxi Province and a possible hydrothermal origin was supposed (Chen and Chen, 1989; Tang et al., 1994; Deng et al., 2003), no unequivocal evidence from REE data and further studies in areas north of Guangxi and farther north were provided. Thus the origin of the basinal chert successions is still uncertain.

The Caledonian basement of South China Block was a coalesced block composed of the Yangtze block (or craton) to the west and the Cathaysia block to the east, as a result of multiphase amalgamation and fragmentation since the Archaean era (e.g., Shui, 1987; Liu et al., 1993). These tectonic activities resulted in a highly inhomogeneous united block, particularly the coupling zone of the two continental blocks (Shui, 1987; Liu et al., 1993), which had a fundamental control on the post-Caledonian evolution. However, it is still unclear when (indeed whether at all) the oceanic crust was evolved between the Yangtze and Cathaysia blocks in the course of re-opening of the coalesced South China block (Hsü et al., 1990; Liu et al., 1993; Zhao et al., 1996; Wu et al., 1998; Li, 2000; Deng et al., 2003; Wu, 2003), which is a key issue of post-Caledonian evolution of the South China block (Liu et al., 1993; Zhao et al., 1996).

In order to improve our understanding for the origin of the Devonian siliceous deposits and their implications for the basin-and-platform tectonics, or to a broader extent, the tectonics of South China block, studies of REE geochemistry upon the siliceous deposits, in the Guilin region, were thus carried out. Our REE data not only support a hydrothermal origin for the chert, in response to the basin-scale, intense basement faulting at depth, but also shed new light on the oceanographic and tectonic scenarios (i.e., open marine) of a broader tectonic regime in South China.

2. Geological setting

After the "Guangxi" (Caledonian) Orogeny, progressive rifting and northeastward transgression from the remnant Qinfang Trough in southern Guangxi (Wu et al., 1987; Liu et al., 1993; Chen et al., 2001a,b) led to the deposition of extensive carbonates on topographic highs (carbonate platforms), and of fine-grained deep-water sediments in the elongate depressions (troughs) in Guangxi–Hunan region during the Givetian (Fig. 1A). Two curvilinear interplatformal basins trending NNE–SSW, located in the western and eastern parts of Guangxi–Hunan region, respectively, extended for about 800 km from Guangxi to Hunan Provinces (Fig. 1A), which generally followed the antecedent basement fault zones (or interplate boundary suture zones) (Liu et al., 1993; Chen et al., 2001b). They are considered as having been formed in response to the reactivation of the principal antecedent basement faults under a sinistral transtensional tectonic setting (Fig. 1B), due to the N–NE migration of the South China block during the Devonian (Wu et al., 1987; Chen et al., 2001b). Two *en echelon* basins trending NE–SW were terminated at the principal, western elongate basin in Guangxi (Fig. 1A, B), and were likely induced by the secondary *en echelon* strike–slip faults (Chen et al., 2001b). The rhomb-shaped basin, trending approximately NW–SE in southern Hunan (Fig. 1A), was considered as a pull-apart basin being formed by the sinistral strike-slip offset by the southern and northern segments of the principal, eastern basement fault zones (Fig. 1B), along which was considered as the trace of suture zone between Yangtze and Cathaysia blocks during the Caledonian orogeny (e.g., Liu et al., 1993). This study focuses on the smaller-scale spindle-shaped Yangshuo Basin in Guilin area (Fig. 1C), which was interpreted as having formed in relation to secondary (sinistral) strike-slip faulting (Fig. 1B–D) (Chen et al., 2001b).

Siliceous sediments were initially deposited in the interplatformal basins from the Early Devonian, episod-

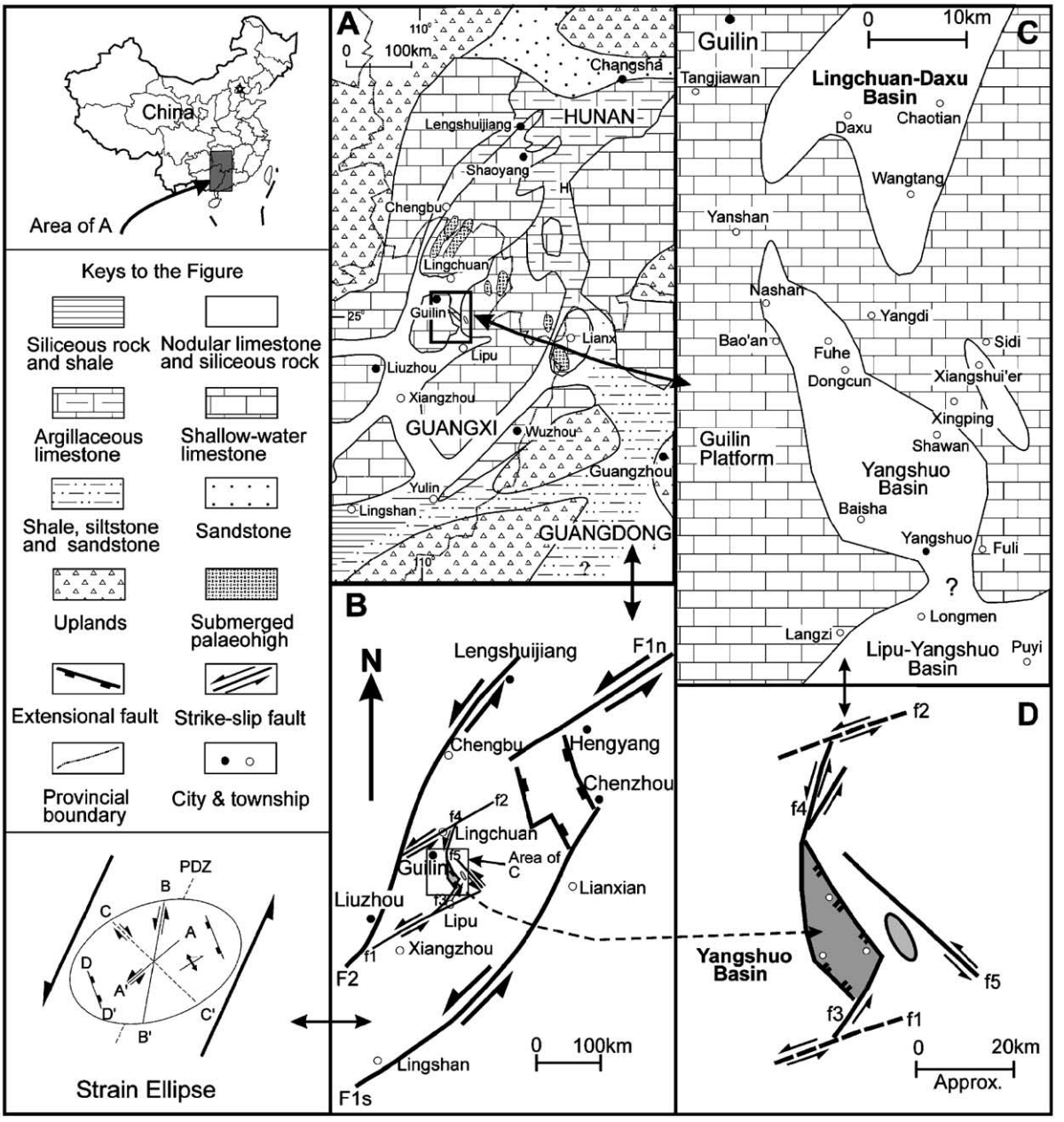

Fig. 1. (A) Paleogeographic setting of the Late Devonian, South China, revealed by the present lithofacies distribution. (B) Structural interpretation of carbonate platform–basin configuration in area of (A) (after Chen et al., 2001b, 2002). Refer to the strain ellipse for the stress regime of the structural style: PDZ, principal displacement zone; A–A′, *en echelon* strike–slip faults; B–B′, synthetic strike–slip faults; C–C′, antithetic strike–slip faults; D–D′, extensional faults. (C) Details of depositional background in the Yangshuo basin, surrounded by carbonate platforms. (D) Structural interpretation for the study area of (C).

ically extending northeastwards later and reaching a maximum extent in the early Late Devonian (Wu et al., 1987). Tuffaceous interbeds are extensive in the chert successions, pillow lava basalts, however, are generally absent except for those occurring in the western Guangxi beyond the study area (e.g., Wu et al., 1987). In the Yangshuo basin, siliceous deposits occur as nodular, bedded and tuffaceous chert in the Liujiang Formation intercalated within basinal carbonate successions of the lower Frasnian (from the *transitans* through

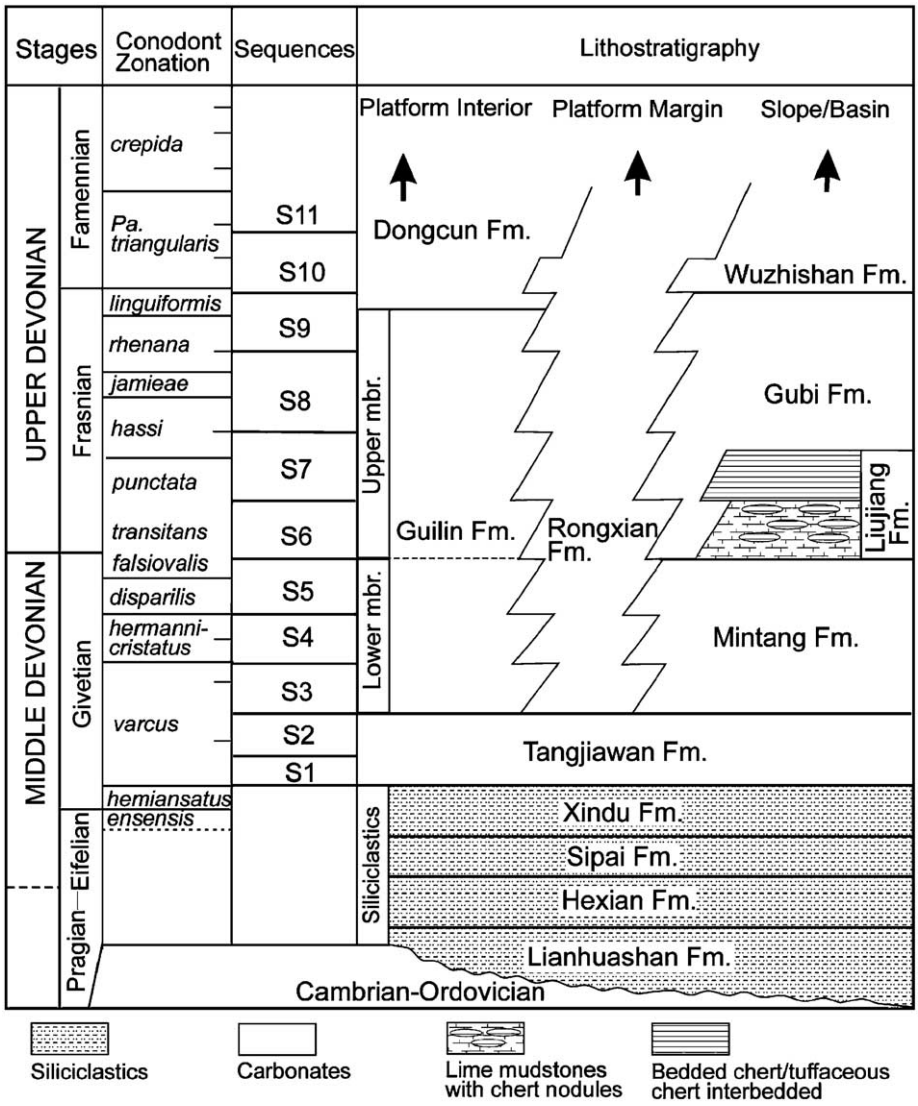

Fig. 2. Lithostratigraphic relationships and nomenclatures for the Devonian platform and basinal successions in Guilin area. The chert deposit is located within the basinal Liujiang Formation. Depositional sequences are documented in Chen et al. (2001b, 2002).

punctata conodont zones) (Fig. 2) (Chen et al., 2001b, 2002). The nodular chert is present in the lower part that is dominated by thin-bedded argillaceous lime mudstones (10 to 20 m thick). It increases upwards volumetrically and grades into black, bedded chert interbeded with brownish to yellownish grey tuffaceous chert, ranging from 2 to 6 cm thick for a single bed, and 15 to 30 m thick for the entire succession. Bedded chert is non-laminated to finely laminated, which also occurs locally as intercalations in the lower carbonate-dominated succession, i.e., at Shawan (see Fig. 1C for location) (Chen et al., 2001b, 2002). The tuffaceous chert has a pumiceous appearance with low density. Minor radiolarians are present both in the bedded and tuffaceous chert, commonly with a better preservation in the latter.

3. Sampling and analytical methodology

Samples of nodular and bedded chert were collected at Shawan, Fuhe and Baisha in the Yangshuo Basin, southeastern Guilin (see Fig. 1C for location), whereas fresh tuffaceous chert was sampled only at the latter two localities in newly cut quarries. All samples were crushed in the steel vessel and further ground to powder in an agate mill.

Major elements were analyzed using an automatic X-ray fluorescence spectrometer (XRF-1500) using fusion glasses made from a mixture of powdered sample and flux ($Li_2B_4O_7$) in the proportion of 1:5. In this study, only results of TiO_2 (reproducibility <0.006 wt.%, same in the brackets below), Al_2O_3 (<0.04 wt.%) and total iron as Fe_2O_3 (<0.13 wt. %) are reported (the Appendix), and $Al_2O_3/(Al_2O_3+Fe_2O_3)$ ratios are used to assess the terrigenous/hydrothermal influxes (Murray, 1994). XRD analysis was conducted to assess the non-silica minerals of the chert.

The sample splits (100 mg) for REE analysis were toasted in an oven at 105 °C for 1–2 h and cooled to room temperature, then digested in a tightly sealed Teflon screw-cap beaker with ultrapure 0.5 ml HNO_3+2.5 ml HF+0.5 ml HClO4, then dried. The dried sample was digested again with 1 ml HNO_3+3 ml H_2O until a clear solution was obtained. The solution was diluted to 1:1000 by mass and analyzed on a VG PQ2 Turbo inductively coupled plasma source mass spectrometer (ICP-MS) at the Institute of Geology and Geophysics, Chinese Academy of Sciences. The precision of the analysis is generally <4% of reported REEs.

Cerium (Ce/Ce*) and europium anomalies (Eu/Eu*) were calculated from: $Ce/Ce^*=Ce_n/(La_n\times Pr_n)^{1/2}$, $Eu/Eu^*=Eu_n/(Sm_n\times Gd_n)^{1/2}$ (Taylor and McClennan, 1985), using shale-normalized abundances. Normalization values are a mean of North American, European and Russian shale composites (Sholkovitz, 1988; Murray et al., 1991). Shale-normalized La_n/Yb_n ratios are assigned to reflect the relative enrichment of light REE (LREE) vs. heavy REE (HREE). La_n/Ce_n ratios (Murray, 1994) are also used in this study to differentiate the depositional environment of chert. La abundances are here used to reflect the total REE contents (ΣREE) as well, in view of their coherent variations with REEs and easy accessibility by different analytical methods.

4. Results

Both nodular and bedded chert has very low TiO_2 (0.01–0.05%) and Al_2O_3 (0.15–1.29%) contents, and high total iron contents as Fe_2O_3 (generally 2.11–3.68%) except for one transitional sample to tuffaceous chert. By contrast, the tuffaceous chert has relatively high TiO_2 (0.10–0.27%) and Al_2O_3 contents (2.31–5.10%), but lower Fe_2O_3 contents (0.93–2.33%) (the Appendix). The $Al_2O_3/(Al_2O_3+Fe_2O_3)$ ratios are extremely low both in nodular and bedded chert (0.04–0.31 generally) and relatively high in the tuffaceous chert (0.58–0.78) (the Appendix). XRD analysis shows almost pure silica (quartz) in the chert, except for extremely weak peaks of muscovite in some samples of tuffaceous chert (Fsi-5, Fsi-6 and Bsi-5).

The shale-normalized relative REE abundance patterns generally indicate an increase of ∑REE from the nodular, to the bedded and tuffaceous chert (Table 1; Fig. 3). All REE patterns display intermediate negative Ce anomalies; those at Shawan and Fuhe are particularly apparent. Moderate to high positive Eu anomalies are also present in some samples, particularly in bedded chert from Shawan and Fuhe (Fig. 3A–B). Comparatively, the positive Eu anomalies are less pronounced at Baisha (Fig. 3C). In general, bedded chert at Shawan exhibits apparent convex REE patterns, whereas those at Fuhe and Baisha commonly have slight gradient REE patterns, particularly in some of the bedded chert from Baisha (Fig. 3).

The La abundances, an indicator of ΣREE variations, are generally low in the nodular chert (1.13–3.29 ppm, avg. 2.07 ppm), are variable, but slightly higher in bedded chert (0.41–5.49 ppm, avg. 2.49), and much higher in the tuffaceous chert (6.78–28.88 ppm, avg. 17.11 ppm) (Table 1; Fig. 4A). The Ce/Ce* ratios vary from 0.56 to 0.89 (avg. 0.69) in nodular chert, from 0.41 to 0.74 (avg. 0.61) in bedded chert, and from 0.56 to 0.72 (avg. 0.63) in tuffaceous chert, indicating an intermediate negative Ce anomaly in all three types of chert (Fig. 4B). Although the La_n/Ce_n ratios of all the chert vary from 1.17 to 2.60, they mostly cluster around 1.70 (Table 1; Fig. 4C). The Eu/Eu* values are from 0.90 to 2.13 (avg. 1.33) in nodular chert, from 1.08 to 2.82 (avg. 1.57) in bedded

Table 1
Variations of La abundance, ΣREE, Ce/Ce*, Eu/Eu*, La_n/Yb_n and La_n/Ce_n in chert

Lithology	La (ppm)	∑REE (ppm)	Ce/Ce*	Eu/Eu*	La_n/Yb_n	La_n/Ce_n
Nodular chert	1.13–3.29	5.82–11.05	0.56–0.89	0.90–2.13	0.75–1.12	1.17–2.13
(n=4)	(avg. 2.07)	(avg. 9.14)	(avg. 0.69)	(avg. 1.33)	(avg. 0.86)	(avg. 1.61)
Bedded chert	0.41–5.49	5.25–23.23	0.41–0.78	1.08–2.82	0.04–0.92	1.26–2.60
(n=12)	(avg. 2.49)	(avg. 12.62)	(avg. 0.61)	(avg. 1.57)	(avg. 0.52)	(avg. 1.72)
Tuffaceous chert	6.78–28.88	44.92–115.11	0.56–0.72	0.88–1.13	0.21–0.69	1.53–2.00
(n=6)	(avg. 17.11)	(avg. 74.55)	(avg. 0.63)	(avg. 0.97)	(avg. 0.48)	(avg. 1.77)

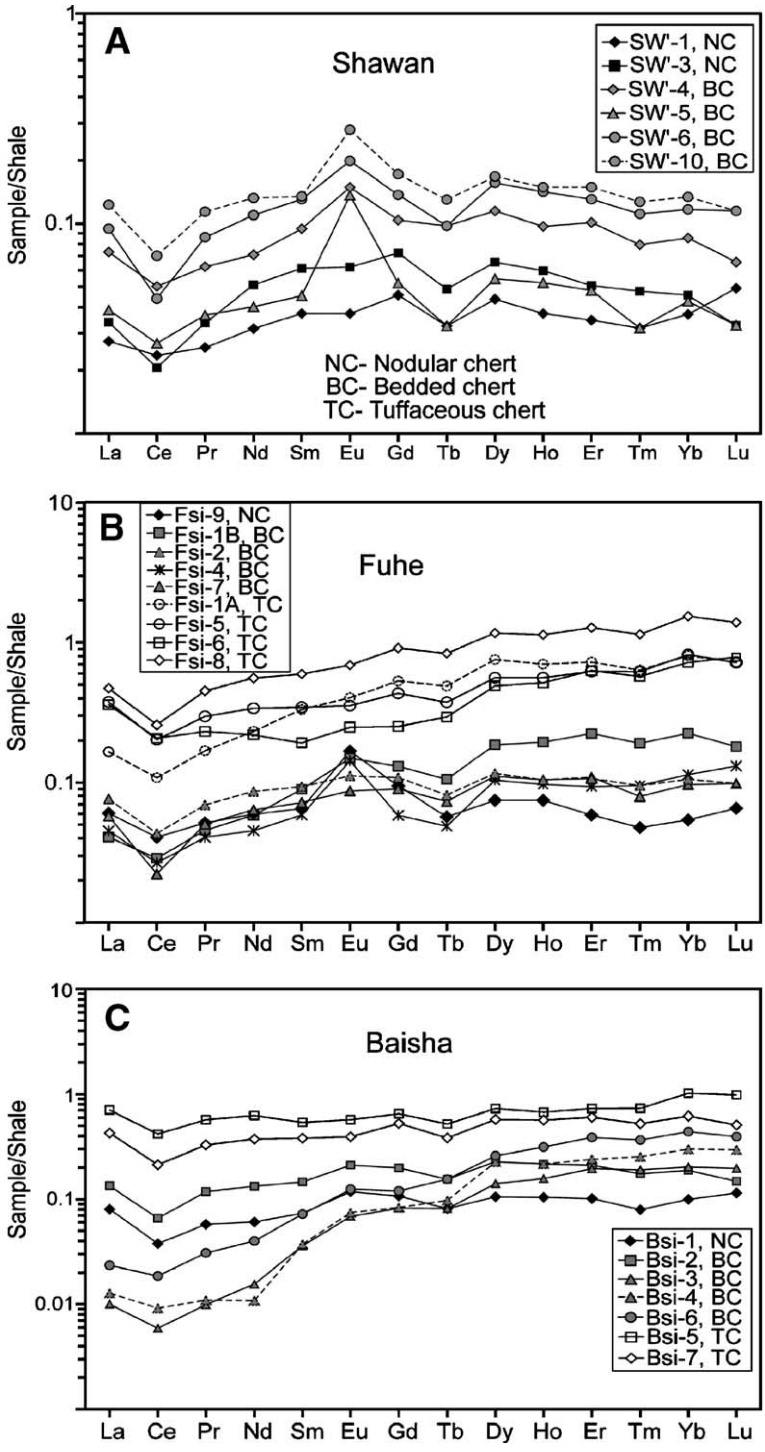

Fig. 3. Shale-normalized REE abundance patterns of different types of chert (nodular, bedded and tuffaceous chert), respectively at Shawan (A), Fuhe (B) and Baisha (C) (see Fig. 1C for location). All the chert shows an intermediate negative Ce anomaly. The tuffaceous chert generally contains the highest total REE contents. At Shawan, the chert (especially bedded cherts) mostly displays apparent positive Eu anomalies, which attenuated at Fuhe and Baisha in order. The systematic Tb depletions in these samples are likely caused by the high Tb value of the shale composite for normalization (Murray et al., 1991).

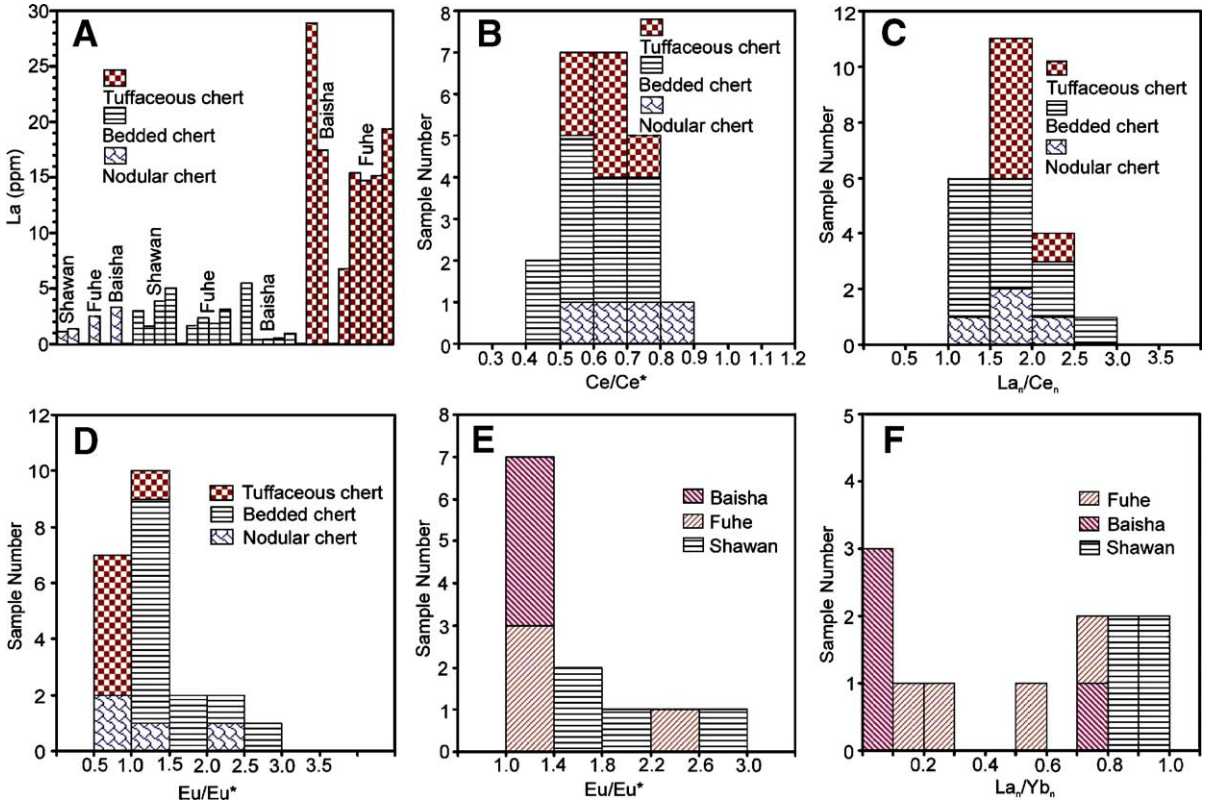

Fig. 4. Histograms showing La abundances (A), Ce/Ce* variations (B) and La_n/Ce_n ratios (C) in different types of chert. Histograms of Eu/Eu* ratios in chert (D) and in bedded chert at studied three localities (E), respectively. (F) Histogram of La_n/Yb_n ratios in bedded chert at studied localities.

chert, and from 0.88 to 1.13 (avg. 0.97) in tuffaceous chert (Table 1; Fig. 4D). These ratios (particularly those in the bedded chert) are variable from place to place, the highest at Shawan and the lowest at Baisha (Fig. 4E). The La_n/Yb_n ratios are mostly less than 1.00 in the three lithologic types except for one high value of 1.12 (Eu/Eu*=2.13 also) in the nodular chert at Fuhe (the Appendix). In the bedded chert, La_n/Yb_n ratios are generally higher at Shawan and lower at Fuhe and Baisha (Fig. 4F).

5. Discussions

5.1. Tectono-sedimentary contexts

Rivers are the main source of REEs to the ocean, and strongly influence the REE chemistry of continental shelf seawaters. Terrigenous materials and water masses derived from continents generally exhibit no apparent fractionation of LREEs from HREEs, and mostly exhibit positive Ce anomalies (e.g., Sholkovitz, 1988, 1990). Negative Ce anomalies have been found mostly within the ocean basins since seawater is typically depleted in Ce due to the preferential removal of Ce^{4+} from the water column (Elderfield and Greaves, 1982) and likely sinking in manganese nodules in view of their positive Ce anomalies (e.g., Fleet, 1983). The Ce/Ce* values were proven fairly consistent during diagenesis (Murray et al., 1992), thus are valuable to identify the depositional environment of chert (or fine-grained sediments) in marine basins (e.g., Murray et al., 1990, 1991; Ding and Zhong, 1995).

Previous studies (Murray et al., 1990, 1991) show that chert sediments deposited near ocean spreading ridges have the lowest Ce/Ce* values (avg. 0.29), while those deposited on the ocean basin floor have the intermediate Ce/Ce* values (avg. 0.60), and those deposited on continental margins have the highest Ce/Ce* values (avg. 1.03) (Table 2). Our Ce/Ce* values (0.41−0.89) from chert are generally consistent with those of an ocean basin environment as stated above (compare Tables 1 and 2; Fig. 4B), suggesting that the chert was deposited in an envi-

Table 2
REE indices of chert formed in different depositional settings (summarized from Murray et al., 1991)

Setting	La (ppm)	∑REE (ppm)	Ce/Ce*	Eu/Eu*	La_n/Yb_n	La_n/Ce_n
Spreading ridge	2.6–106 (avg. 27.2)	10.9–406 (avg. 107.96)	0.18–0.6 (avg. 0.29)	0.97–1.35 (avg. 1.08)	0.57–0.96 (avg. 0.74)	1.66–5.49 (avg. 3.59)
Open-ocean basin	2.81–30.6 (avg. 16.31)	14.3–108 (avg. 57.2)	0.5–0.76 (avg. 0.6)	1.06–1.33 (avg. 1.15)	0.48–2.26 (avg. 1.30)	1.30–2.48 (avg. 1.82)
Continental margin	1.2–27.91 (avg. 8.34)	7.9–152.2 (avg. 49.33)	0.67–1.52 (avg. 1.11)	0.64–1.72 (avg. 1.21)	0.43–1.22 (avg. 0.75)	0.66–1.33 (avg. 0.96)

ronment significantly far from terrigenous sources, i.e., in an open marine basin (this term rather than ocean basin is used due to lack of submarine basalts in this region). This scenario is further demonstrated by the intermediate to high La_n/Ce_n values that mainly cluster between 1.5 and 2.0 (Fig. 4C), which are also in a good agreement with the values of open ocean basins (1.0–2.5) proposed by Murray (1994). The shale-normalized La_n/Yb_n ratios of chert (mostly <0.9, Table 1) generally indicate a LREE-depleted pattern, although a spatial variation of these values does occur (see later discussion), suggesting a preferential removal of LREEs relative to HREEs in seawater (cf. Elderfield and Greaves, 1982). This could have not occurred if significant amount of terrigenous particulates (La_n/Yb_n: 1.0 to 1.3; (Sholkovitz, 1990; Condie, 1991) were delivered to the sea. This further suggests an open marine condition far from the terrigenous inputs during the precipitation of the chert in the study area.

This scenario, to a broader extent, implies that the Guangxi–Hunan region (inboard Huanan block) (Hsü et al., 1990) might have quickly evolved from an intracontinental rift basin starting from the Early Devonian into an open marine (rift) basin with a reasonable size in the early Late Devonian, which was assumed to having not been occurred in this region until the Carboniferous–Permian time in previous studies (e.g., Liu et al., 1993; Zhao et al., 1996; Wu et al., 1998; Wu, 2003). Under this circumstance, the two elongate interplatform basin (or trough) systems, both east and west of the study area (Fig. 1A), could have been much wider than presently preserved widths (10−60 km commonly), such that the terrigenous materials sourced from the Jiangnan (or Xuefengshan) upland to the west and the Cathaysia (or Wuyi–Yunkai) upland to the east (cf. Hsü et al., 1990; Liu et al., 1993) were mostly entrapped by the elongate basin systems and barely reached the study area (Fig. 1A). Nevertheless, more REE data of the Devonian chert successions in larger areas are necessary to attest the paleoceanographic and tectonic scenarios of South China block revealed by this study. The presence of tuffaceous interbeds in the siliceous section indicates simultaneous volcanic activity during the chert deposition.

5.2. Hydrothermal activity

Eu^{2+} commonly occurs in a strongly reduced environment related to magmatic processes within the lower crust or with a significant contribution of detrital feldspar minerals (Taylor and McClennan, 1985). It does not seem to have appeared within ocean basins except in the hydrothermal system (giving the positive Eu anomalies) (Michard et al., 1983; German et al., 1990, 1999), as a result of crystochemical exchange with plagioclase phenocrysts formed in the vent and speciation of vent fluids (Douville et al., 1999). Typically, sediments precipitated from vent fluids yield pronounced positive Eu anomalies, with little or no negative Ce anomaly (e.g., German et al., 1990). Although there are large hydrothermal Eu inputs to the ocean as stated above, rare apparent positive Eu anomalies and relatively LREE-enriched patterns (compared with the typical LREE-depleted pattern of seawater) are well documented in siliceous sediments in geological records (e.g., Murray et al., 1991).

Positive Eu anomalies (Figs. 3A–B and 4D–F) with convex REE patterns, particularly in the bedded chert from Shawan and Fuhe, are similar to those reported in the modern ocean ridge vent fluids and associated hydrothermal sediments (Michard et al., 1983; Michard, 1989; German et al., 1990, 1999), suggesting a strong influence from hydrothermal fluids (Douville et al., 1999). Although a contribution of detrital feldspar minerals can also lead to the positive Eu anomalies (Owen et al., 1999), no detection of them in the chert by XRD analysis excludes this possibility. Accordingly, the decreasing of positive Eu anomalies and systematic variations of

REE patterns from Shawan, to Fuhe and to Baisha (Fig. 3) likely points to an attenuation of hydrothermal activity and an enhanced influence of seawater (cf., German et al., 1990). The decrease of La_n/Yb_n values from Shawan to Fuhe and Baisha (Fig. 4F), particularly in the bedded chert, indicates reduced abundances of LREE vs. HREE in this trend. This, in turn, suggests a decrease of hydrothermal activity and an increasing influence of seawaters along this trend since most vent fluids (i.e., high-temperature, Cl-rich acid solutions, PH=4–6) show REE patterns with relative LREE enrichment and positive Eu anomaly (Michard et al., 1983; Michard, 1989; German et al., 1990, 1999; Douville et al., 1999). Although some high-temperature, SO_2-rich acid vent fluids can result in LREE-depleted patterns with no pronounced Eu anomalies due to removal of LREEs by SO_4-complexation and oxidation of hydrothermal fluids (Douville et al., 1999), the absence of sulfates (i.e., barites and/or anhydrites) in the chert section at Baisha, however, reduces the possibility that the depleted LREE pattern lack of a pronounced Eu anomaly (Figs. 3C and 4F) was caused by SO_2-rich vent fluids. The chert deposits with both negative Ce and positive Eu anomalies indicate that their formation was involved with both seawaters and hydrothermal vent fluids, similar to the case of modern ocean hydrothermal systems (e.g., German et al., 1990, 1999).

Studies show ∑REE/Fe ratios of hydrothermal sediments increase with increasing distance away from the active hydrothermal vents (Ruhlin and Owen, 1986; Olivarez and Owen, 1989; Murray et al., 1991). The approximate inverse dependence of ∑REE on Fe contents in the siliceous deposits (Fig. 5), that is, an increase of ∑REE/Fe from nodular and bedded chert to tuffaceous chert, suggests the adsorption from seawater were the dominant source of REEs to the siliceous deposits. As such, a high precipitation rate of silica matter in the hydrothermal vent systems could have limited the residence time of sediment particles in seawater, therefore, less REEs were then absorbed upon the siliceous sediments (Ruhlin and Owen, 1986; Olivarez and Owen, 1989; Murray et al., 1991). The low La abundances, thereby low ∑REE contents (Figs. 4A and 5), both in nodular and bedded chert (Table 1) were thus likely resulted mainly from their high precipitation rates, and/or the scavenging of REE by Fe–Mn oxyhydroxides in the hydrothermal vent systems (e.g., German et al., 1990; Olivarez and Owen, 1989). Nevertheless, other causes that resulted in the depletion of REEs, i.e., diagenetic siliceous dilution (Murray et al., 1991), cannot be unambiguously excluded for some of the chert since ∑REE in a few samples are independent from the variations of Fe contents (Fig. 5). Moreover, the lower La and ∑REE contents (Table 1) in the nodular chert may have also succeeded the REE pattern of the deep-water marine limestones that generally contain very a low ∑REE concentration (Taylor and McClennan, 1985). The La and ∑REE contents in tuffaceous chert are relatively high (Table 1), and approximately fall within the range of tuffs that commonly have

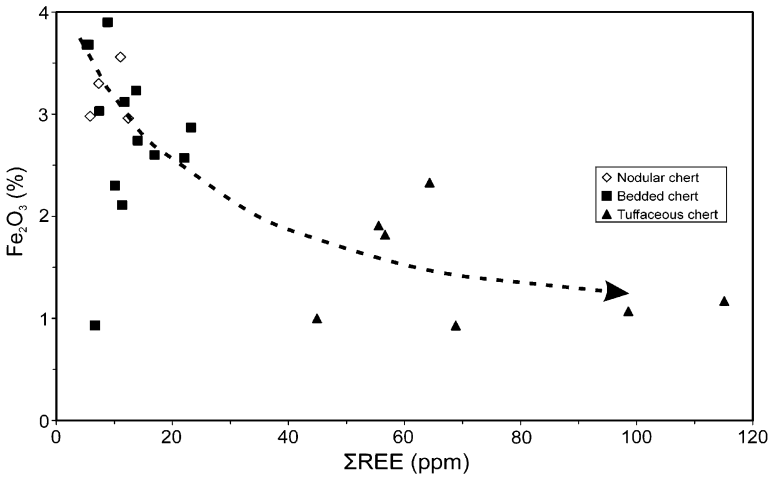

Fig. 5. Crossplot of ∑REE and Fe_2O_3 (total Fe) contents in different types of chert. An approximate negative relationship is present between them (arrow), especially for bedded and tuffaceous chert.

negative Eu anomalies (e.g., Song et al., 2000; Risso et al., 2002). Their negative Ce anomalies and absence of Eu anomalies (Table 1; Figs. 3 and 4) were likely caused by the hydrothermal alteration upon the tuffaceous fallouts, otherwise they would have positive Ce and negative Eu anomalies.

It is noted that both nodular and bedded chert have consistent high Fe concentrations (Fig. 5) and very low Al_2O_3 and TiO_2 concentration, and low $Al_2O_3/(Al_2O_3+Fe_2O_3)$ ratios except for transitional samples to tuffaceous chert (the Appendix), pointing to an apparent hydrothermal influence (Adachi et al., 1986) for all. Nevertheless, this scenario is not the case revealed by REE geochemistry, as documented earlier. The systematic, but rapid spatial change of REE pattern and Eu/Eu* ratios in siliceous

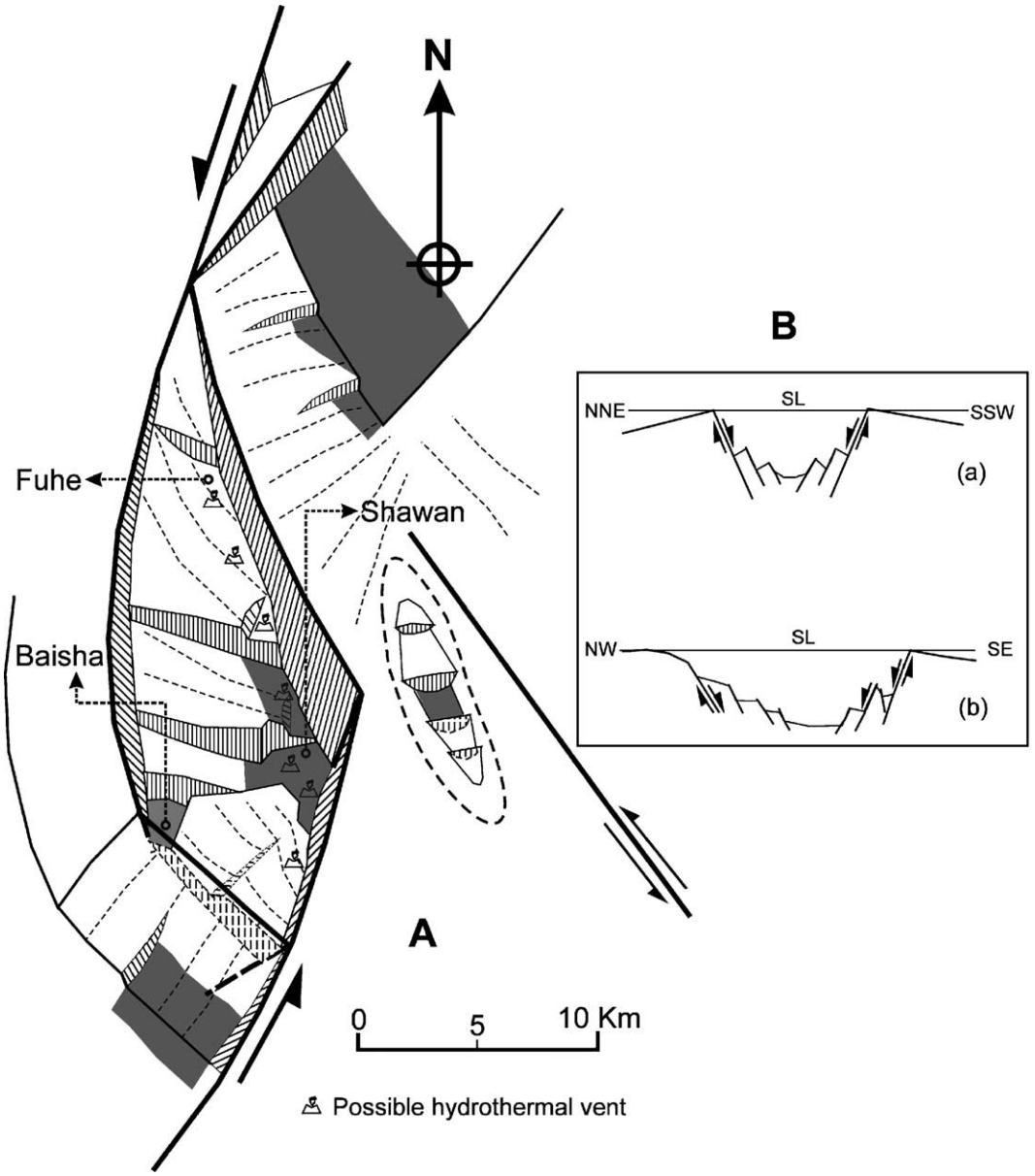

Fig. 6. (A) Schematic diagram showing the asymmetrical spindle-shaped geometry and tectonic pattern of the Yangshuo basin. Dark areas reflect the relative deep centres, which are diagonally arranged in the distal part of the master fault zones. Note the possible distribution of hydrothermal vents. (B) Schematic cross-section showing the (a) axial and lateral geometry of the Yangshuo basin (modified from Chen et al. 2001b).

deposits illustrates that only those precipitated very much close to the active hydrothermal vent (<10 km in distance typically; see Figs. 1C and 6) can evidence of LREE enrichment and apparent positive Eu anomalies characteristic of hydrothermal venting be recorded (Fig. 3), which may account for the paradox of why rare hydrothermal characteristics (LREE enrichment and positive Eu anomaly) were well reported in chert in geological records (Murray et al., 1991). This discrepancy indicates that the REE geochemistry can locate the ancient active hydrothermal vent systems more accurately than the major element geochemistry can do.

5.3. Implications for basin infrastructure

The spatial variation of hydrothermal activity, as documented above, could have also been a reflection of intensity of basement tectonic activity in the studied Yangshuo basin. This basin was interpreted as a pull-apart basin induced by the secondary sinistral strike–slip faulting under a larger transtensional tectonic regime (Figs. 1B–D and 6), based on tectono-sedimentay analysis (Chen et al., 2001b). Under such circumstances, the most intense, deep-seated faulting, which could have channeled hydrothermal fluids from depth to the seafloor, took place at Shawan (Figs. 1C, D and 6), where the chert has more pronounced Eu anomalies with lower degree of LREE depletion (Fig. 3A). Accordingly, relatively mild faulting with a lesser influence of hydrothermal fluids occurred at Baisha where the chert has no apparent Eu anomaly but a more pronounced LREE-depleted pattern (Fig. 3C) typical of seawater signatures (Elderfield and Greaves, 1982). This interpretation further reconciles the scenario of a pull-apart basin induced by strike–slip faulting, where Shawan and Baisha were located, respectively at the distal part (maximal tensional stress area) of the active and the passive master faults; Fuhe area, on the other hand, was located along the oblique extensional fault that linked the two master faults (Figs. 1C, D and 6) (cf. Chen et al., 2001b). In this case, the stronger deep-seated, strike–slip basement faulting along the eastern active master fault zone could have created a stronger extensional regime at the distal part of this zone (Mann et al., 1983), i.e., at Shawan (Chen et al., 2001b), allowing the hydrothermal fluids at depth to move upwards to the seafloor substantially there. By contrast, a relatively mild extensional regime likely created at the distal part of the passive master fault zone (Mann et al., 1983), i.e., at Baisha (Chen et al., 2001b), so relatively mild hydrothermal activity occurred there (Fig. 6).

6. Conclusions

The intermediate Ce anomalies (Ce/Ce^*: ~0.6), intermediate to high La_n/Ce_n ratios (1.5−2.0 mostly), and low to intermediate La_n/Yb_n ratios (0.04−1.12) in the siliceous deposits of Late Devonian in the study area suggest that they were formed in an open marine regime that was significantly far away from the terrigenous sources. The extremely low La (thereby $\sum$REE) abundances and convex REE patterns with positive Eu anomalies and less LREE-depletions in some of the nodular and bedded chert point to a hydrothermal origin for the chert, with significant REEs contributed from hydrothermal fluids. The spatially systematic variations of the REE patterns and Ce–Eu anomalies accordingly reflects the interactions and differential influences of seawater and hydrothermal fluids. The spatial variations of hydrothermal activity could further have been a reflection in the differential intensity of (transtensional) tectonic activity in the study area, where deep-seated faulting could have led to prominent hydrothermal venting (with apparent positive Eu anomalies) on the seafloor, and vice versa. The hydrothermal venting was concurrent with volcanic activity in the Late Devonian in South China, as demonstrated by the tuffaceous beds in the siliceous successions. Detailed spatial studies on REE geochemistry of siliceous deposits, therefore, can provide unique information to delineate the ancient active hydrothermal vent systems, thereby unraveling the tectonic scenario of sedimentary basins.

Acknowledgements

This work was supported by the National Key Basic Research Project of China through Grant 2005CB422101 and the National Natural Science Foundation of China (NSFC) through Grant 40372062. Many thanks go to Bao'an Yin, Hongjin Lu and many colleagues from the Regional Geological Survey and Research of Guangxi Autonomous Region for their helps during the fieldwork. Constructive comments from R.W. Murray and an anonymous reviewer, and Editor B.W. Sellwood are highly appreciated.

Appendix A. Summary of TiO_2, Al_2O_3 and F_2O_3 contents (wt.%), REE concentration (ppm) in the chert of Late Devonian, Guilin area, South China

Locality/ Sample	TiO_2	Al_2O_3	$Fe_2O_3^{\#}$	Al/(Al+Fe)	La	Ce	Pr	Nd	Sm	Eu	Gd	Tb	Dy	Ho	Er	Tm	Yb	Lu	∑REE	Ce/Ce*	Eu/Eu*	La_n/Yb_n	La_n/Ce_n
Shale composite*					41.00	83.00	10.10	38.00	7.50	1.61	6.35	1.23	5.49	1.34	3.75	0.63	3.51	0.61	204.15	1	1	1	1
Shawan																							
SW′-1, NC	0.02	0.31	2.98	0.09	1.13	1.96	0.26	1.20	0.28	0.06	0.29	0.04	0.24	0.05	0.13	0.02	0.13	0.03	5.82	0.89	0.90	0.74	1.17
SW′-3, NC	0.01	0.15	3.30	0.04	1.39	1.71	0.34	1.94	0.46	0.10	0.46	0.06	0.36	0.08	0.19	0.03	0.16	0.02	7.30	0.61	0.93	0.74	1.65
SW′-4, BC	0.03	0.59	3.23	0.15	3.00	4.17	0.63	2.70	0.71	0.24	0.66	0.12	0.63	0.13	0.38	0.05	0.30	0.04	13.76	0.74	1.50	0.86	1.46
SW′-5, BC	0.02	0.42	3.03	0.12	1.59	2.24	0.37	1.53	0.34	0.22	0.33	0.04	0.30	0.07	0.18	0.02	0.15	0.02	7.40	0.72	2.82	0.91	1.44
SW′-6, BC	0.03	0.68	2.6	0.21	3.88	3.65	0.87	4.17	0.98	0.32	0.87	0.12	0.86	0.19	0.49	0.07	0.41	0.07	16.95	0.49	1.49	0.81	2.15
SW′-6-R					4.28	4.12	0.99	4.47	0.94	0.40	1.03	0.17	0.90	0.19	0.48	0.08	0.48	0.07	18.60	0.49	1.74	0.76	2.10
SW′-10, BC	0.05	1.04	2.57	0.29	5.04	5.83	1.15	5.03	1.01	0.45	1.09	0.16	0.92	0.20	0.56	0.08	0.47	0.07	22.06	0.59	1.84	0.92	1.75
Baisha																							
Bsi-1, NC	0.03	0.63	2.96	0.18	3.29	3.13	0.58	2.30	0.55	0.19	0.68	0.10	0.58	0.14	0.38	0.05	0.35	0.07	12.39	0.56	1.33	0.80	2.13
Bsi-2, BC	0.02	0.45	2.87	0.14	5.49	5.46	1.19	5.02	1.09	0.34	1.26	0.19	1.25	0.29	0.79	0.11	0.66	0.09	23.23	0.52	1.24	0.71	2.04
Bsi-3, BC	0.02	0.30	3.68	0.08	0.41	0.49	0.10	0.59	0.27	0.11	0.52	0.10	0.77	0.21	0.73	0.12	0.71	0.12	5.25	0.59	1.26	0.05	1.69
Bsi-3-R	0.02	0.32	3.68	0.08	0.42	0.58	0.09	0.47	0.24	0.17	0.56	0.13	0.86	0.21	0.70	0.14	0.88	0.12	5.57	0.73	1.99	0.04	1.47
Bsi-4, BC	0.05	1.29	0.93	0.58	0.52	0.76	0.11	0.41	0.28	0.12	0.53	0.12	1.24	0.29	0.90	0.16	1.05	0.18	6.67	0.78	1.34	0.04	1.39
Bsi-6, BC	0.04	0.93	2.11	0.31	0.96	1.54	0.31	1.52	0.54	0.20	0.76	0.19	1.42	0.42	1.45	0.23	1.54	0.24	11.32	0.69	1.34	0.05	1.26
Bsi-6-R					0.88	1.63	0.30	1.70	0.47	0.19	0.84	0.18	1.45	0.42	1.30	0.21	1.48	0.24	11.29	0.78	1.30	0.05	1.09
Bsi-5, TC	0.22	4.06	1.17	0.78	28.88	34.64	5.78	23.81	4.04	0.92	4.13	0.64	4.00	0.90	2.73	0.46	3.58	0.6	115.11	0.66	0.97	0.69	1.69
Bsi-7, TC	0.10	2.46	0.93	0.73	17.46	17.64	3.31	14.14	2.85	0.63	3.34	0.47	3.16	0.76	2.26	0.33	2.17	0.31	68.83	0.57	0.88	0.69	2.00
Fuhe																							
Fsi-9, NC	0.03	0.44	3.56	0.11	2.48	3.37	0.52	2.26	0.49	0.27	0.60	0.07	0.41	0.10	0.22	0.03	0.19	0.04	11.05	0.73	2.13	1.12	1.49
Fsi-9-R					2.47	3.40	0.52	2.31	0.45	0.25	0.49	0.07	0.39	0.09	0.26	0.03	0.18	0.03	10.94	0.74	2.28	1.17	1.47
Fsi-1B, BC	0.03	0.54	3.12	0.15	1.67	2.39	0.46	2.22	0.67	0.24	0.83	0.13	1.02	0.26	0.84	0.12	0.79	0.11	11.75	0.67	1.38	0.18	1.41
Fsi-2, BC	0.02	0.24	2.30	0.09	2.36	1.84	0.51	2.43	0.54	0.14	0.57	0.09	0.61	0.14	0.41	0.05	0.34	0.06	10.09	0.41	1.08	0.59	2.60
Fsi-4, BC	0.02	0.51	3.90	0.12	1.85	2.22	0.41	1.72	0.44	0.23	0.37	0.06	0.57	0.13	0.35	0.06	0.40	0.08	8.89	0.62	2.44	0.40	1.69
Fsi-7, BC	0.04	0.74	2.74	0.21	3.13	3.59	0.70	3.28	0.70	0.18	0.69	0.10	0.64	0.14	0.40	0.06	0.37	0.06	14.04	0.59	1.11	0.72	1.76
Fsi-1A, TC	0.12	2.31	1.00	0.70	6.78	9.00	1.70	8.84	2.49	0.65	3.37	0.60	4.16	0.94	2.72	0.40	2.83	0.44	44.92	0.65	0.96	0.21	1.53
Fsi-5, TC	0.18	3.23	2.33	0.58	15.42	16.81	2.99	12.87	2.58	0.57	2.76	0.46	3.07	0.75	2.33	0.39	2.88	0.44	64.32	0.61	0.92	0.46	1.86
Fsi-6, TC	0.27	5.21	1.91	0.73	14.73	17.20	2.34	8.35	1.44	0.40	1.60	0.36	2.69	0.69	2.36	0.36	2.53	0.48	55.53	0.72	1.13	0.50	1.73
Fsi-6-R	0.27	5.10	1.82	0.74	15.17	17.31	2.28	7.93	1.64	0.43	1.75	0.35	2.78	0.76	2.49	0.38	2.93	0.45	56.65	0.72	1.09	0.44	1.77
Fsi-8, TC	0.17	3.64	1.07	0.77	19.36	21.41	4.57	21.15	4.46	1.11	5.80	1.03	6.40	1.52	4.78	0.72	5.41	0.85	98.57	0.56	0.94	0.31	1.83

$Fe_2O_3^{\#}$ =total Fe, Al/(Al+Fe)=$Al_2O_3/(Al_2O_3+Fe_2O_3)$, *—values of the composite of North American, Europian and Russian shales (Sholkovitz, 1988). NC—nodular chert, BC—bedded chert, TC—tuffaceous chert, R—replicate run.

References

Adachi, M., Yamamoto, K., Sugisaki, R., 1986. Hydrothermal chert and associated siliceous rocks from the northern Pacific: their geological significance as indication of ocean ridge activity. Sediment. Geol. 47, 125–148.

Armstrong, H.A., Owen, A.W., Floyd, J.D., 1999. Rare earth geochemistry of Arenic cherts from the Ballantrae Ophiolite and Leadhills Imbricated Zone, southern Scotland: implications for origin and significance to the Caledonian Orogeny. J. Geol. Soc. Lond. 156, 549–560.

Chen, X.P., Chen, D.F., 1989. Geochemistry of Upper Devonian mammiform chert in Guangxi. Geochimica 18, 1–8 (in Chinese with English abstract).

Chen, D., Tucker, M.E., Jiang, M., Zhu, J., 2001a. Long-distance correlation between tectonic-controlled, isolated carbonate platforms by cyclostratigraphy and sequence stratigraphy in the Devonian of South China. Sedimentology 48, 57–78.

Chen, D., Tucker, M.E., Zhu, J., Jiang, M., 2001b. Carbonate sedimentation in a starved pull-apart basin, Middle to Late Devonian, southern Guilin, South China. Basin Res. 13, 141–167.

Chen, D., Tucker, M.E., Zhu, J., Jiang, M., 2002. Carbonate platform evolution from a bioconstructed platform margin to a sand–shoal system (Devonian, Guilin, South China). Sedimentology 49, 737–764.

Condie, K.C., 1991. Another look at rare earth elements in shales. Geochim. Cosmochim. Acta 55, 2527–2531.

Deng, X.G., Li, X.H., Chen, Z.G., 2003. Geochemical features and sedimentary setting of Late Devonian cherts in Bancheng of Qinzhou, Guangxi. Chin. J. Geol. 38, 460–469.

Ding, L., Zhong, D., 1995. Rare earth elements and Ce anomalies in the chert of the Paleo–Tethys Ocean, Changning–Menglian belt, western Yunnan. Sci. China (Series B) 25, 93–100.

Douville, E., Bienvenu, P., Charlou, J.L., Donval, J.P., Fouquet, Y., Appriou, P., Gamo, T., 1999. Yttrium and rare earth elements in fluids from various deep-sea hydrothermal systems. Geochim. Cosmochim. Acta 63, 627–643.

Elderfield, H., Greaves, M.J., 1982. The rare earth elements in seawater. Nature 296, 214–219.

Fleet, A.J., 1983. Hydrothermal and hydrogenous ferro–manganese deposits: Do they form a continuum? The rare earth element evidence. In: Rona, P.A., Boström, K., Laubier, L., Smith, K.L. (Eds.), Hydrothermal Process at Seafloor Spreading Centers. Plenum Press, New York, pp. 535–555.

German, C.R., Klinkhammer, G.P., Edmond, J.M., Mitra, A., Elderfield, H., 1990. Hydrothermal scavenging of rare earth elements in the ocean. Nature 345, 516–518.

German, C.R., Hergt, J., Palmer, M.R., Edmond, J.M., 1999. Geochemistry of a hydrothermal sediment core from the OBS ventfield, 21°N East Pacific Rise. Chem. Geol. 155, 65–75.

Holser, W.T., 1997. Evaluation of the application of rare-earth elements to paleoceanography. Palaeogeogr. Palaeoclimatol. Palaeoecol. 132, 309–323.

Hsü, K.J., Li, J.L., Chen, H.H., Wang, Q.C., Sun, S., Sengör, A.M.C., 1990. Tectonics of South China: key to understanding west Pacific geology. Tectonophysics 183, 9–39.

Li, X.H., 2000. Geochemistry of the Late Paleozoic radiolarian cherts within the NE Jiangxi ophiolite mélange and its tectonic significance. Sci. China (Ser. D) 43, 617–624.

Liu, B.J., Xu, X.S., Pan, S.N., Huang, H.C., 1993. Sedimentary–Crustal Evolution and Mineralization of the Paleo-continent of South China. Science Press, Beijing. 236 pp.

Mann, P., Hempton, M.R., Bradley, D.C., Burkle, K., 1983. Development of pull-apart basins. J. Geol. 91, 529–554.

Michard, A., 1989. Rare earth element systematics in hydrothermal fluids. Geochim. Cosmochim. Acta 53, 745–750.

Michard, A., Albarède, G., Michard, G., Minster, J.F., Charlou, J.L., 1983. Rare-earth elements and uranium in high-temperature solutions from East Pacific Rise hydrothermal vent field (13°N). Nature 303, 795–797.

Murray, R.W., 1994. Chemical criteria to identify the depositional environment of chert: general principles and applications. Sediment. Geol. 90, 213–232.

Murray, R.W., Buchholtz ten Brink, M.R., Jones, D.L., Gerlach, D.C., Russ III, G.P., 1990. Rare earth elements as indicators of different marine depositional environments in chert and shale. Geology 18, 268–271.

Murray, R.W., Buchholtz ten Brink, M.R., Gerlach, D.C., Russ III, G.P., Jones, D.L., 1991. Rare earth, major, and trace elements in chert from the Franciscan complex and Monterey group, Californian: assessing REE sources to fine-grained marine sediments. Geochim. Cosmochim. Acta 55, 1875–1895.

Murray, R.W., Buchholtz ten Brink, M.R., Gerlach, D.C., Russ III, G.P., Jones, D.L., 1992. Rare earth, major, and trace element composition of Monterey and DSDP chert and associated host sediment: assessing the influence of chemical fractionation during diagenesis. Geochim. Cosmochim. Acta 56, 2657–2671.

Olivarez, A.M., Owen, R.M., 1989. REE/Fe variations in hydrothermal sediments: implications for the REE content of seawater. Geochim. Cosmochim. Acta 53, 757–762.

Owen, A.W., Armstrong, H.A., Floyd, J.D., 1999. Rare earth elements in chert clasts as provenance indicators in the Ordovician and Silurian of the Southern Uplands of Scotland. Sediment. Geol. 124, 185–195.

Risso, C., Scasso, R.A., Aparicio, A., 2002. Presence of large pumice blocks on Tierra del Fuego and South Shetland Islands shorelines, from 1962 South Sandwich Islands eruption. Mar. Geol. 186, 413–422.

Ruhlin, D.E., Owen, R.M., 1986. The rare earth element geochemistry of hydrothermal sediments from the East Pacific Rise: examination of seawater scavenging mechanism. Geochim. Cosmochim. Acta 50, 393–400.

Shimizu, H., Masuda, A., 1977. Cerium in chert as an indication of marine environment of its formation. Nature 266, 346–348.

Sholkovitz, R.E., 1988. Rare earth elements of the North Atlantic Ocean, Amazon Delta, and East China Sea: reinterpretation of terrigenous input patterns to the ocean. Am. J. Sci. 288, 236–281.

Sholkovitz, E.R., 1990. Rare earth elements in marine sediments and geochemical standards. Chem. Geol. 88, 333–347.

Shui, T., 1987. Tectonic framework of the continental basement of southeastern China. Sci. China (SerB) 17, 414–422 (in Chinese).

Song, S.-R., Chen, C.H., Lee, M.-Y., Tang, T.F., Iizuka, Y., Wei, K.-Y., 2000. Newly discovered eastern dispersal of the Youngest Toba Tuff. Mar. Geol. 167, 303–312.

Tang, S.R., Liu, W.J., Luan, S.W., 1994. Characteristics of cherts in the Xialei manganese ore mining area and their origin. Sci. Geol. Sinica (Overseas Edition) 3, 59–71.

Taylor, S.R., McClennan, S.M., 1985. The Continental Crustal: Its Composition and Evolution. Blackwell, Oxford. 312 pp.

Wu, H.R., 2003. Discussion on tectonic palaeogeography of Nanpanjiang sea in the Late Paleozoic and Triassic. J. Palaeogeogr. 5, 63–76.

Wu, Y., Zhou, H.L., Jiang, T.C., Fang, D.N., Huang, W.S., 1987. The Sedimentary Facies, Palaeogeography and Relative Mineral Deposits of the Devonian in Guangxi. Guangxi People's Publishing House, Nanning, China. 292 pp.

Wu, F.Y., Sun, J.P., Zhang, X.Z., 1998. The Nd isotopic evidence for Late Paleozoic oceanic crust in southern margin of Yangtze block. Acta Petrol. Sinica 14, 22–33.

Zhao, C.H., He, K.Z., Zhou, Z.G., Le, C.S., Nie, Z.T., Tai, D.Q., Ye, N., 1996. New understanding on geotectonic problems in South China block. Geoscience-J. Grad. Sch., China Univ. Geosci. 10, 512–517 (in Chinese with English abstract).